



# Magnetic properties of surface sediments from Liuxi River, southern China and their environmental significance

Erqi Zheng<sup>1</sup> · Yang Bai<sup>2</sup> · Mingkun Li<sup>1</sup> · Tingping Ouyang<sup>1</sup> · Fangzhi Zhang<sup>2</sup> · Mingjie Yu<sup>1</sup> · Gang Lei<sup>2</sup> · Zhiyi Pan<sup>1</sup> · Gang Long<sup>3</sup>

Received: 6 October 2021 / Accepted: 28 January 2022 / Published online: 10 February 2022  
© The Author(s), under exclusive licence to Springer-Verlag GmbH Germany, part of Springer Nature 2022

## Abstract

**Purpose** Magnetic minerals within fluvial sediments are affected by a variety of natural and anthropogenic factors, limiting the capability of sediment magnetism in tracing provenance, assessing pollution, and other environmental or geological fields.

**Methods** Twenty-three samples were collected from Liuxi River, a river influenced by complex natural and human processes, in southern China to conduct the analysis of magnetism, particle size, and geochemical elements. The micromorphology of magnetic particles was directly observed by scanning electron microscope and energy dispersive spectrometer.

**Results** The following are the factors affecting the sediment magnetic properties: (1) There is a sampling site in the upper reach with over 100 times magnetic susceptibility than other sites. This sampling site is close to the areas having documented iron ore mining and smelting activities in the past few hundred years, and the sample contains the very high concentrations of metals (e.g., Fe, Mn, Ni, Pb, Sn, V, Cr, Cu, and Bi), implying the ancient mining activity could pose environmental risks in modern sediments. (2) In a downstream direction, magnetic concentration shows a decreasing tendency and magnetic grain size becomes finer. The contributions of superparamagnetic particles and high-coercivity minerals (e.g., hematite) to the total magnetism increase, and technogenic magnetic particles appear downstream of urban areas. In general, the upstream magnetic minerals are controlled by weakly weathered coarse-grained particles produced by granite denudation, while the downstream magnetic minerals are affected by the sedimentary rocks and the human activity. (3) Magnetic minerals become coarse after the river flows over barrages in response to the hydrodynamic changes.

**Conclusions** The investigation reveals the natural and anthropogenic influences according to the analysis of the sediments in Liuxi River, and further research related to the sediment magnetism in complex river should be conducted.

**Keywords** Southern China · Magnetic parameters · Ancient mining · Human activities

## 1 Introduction

As one of the most active systems on the Earth's surface, rivers play a critical role in linking mountains and coastal areas, eroding the earth surface, and transporting terrestrial materials and nutrients to the oceans (Steffen et al. 2006; Milliman and Farnsworth 2011). River sediment properties, called “fingerprints” are employed to study the erosion in drainage basins, sediment discharge, and provenance in the catchment and marginal seas. However, due to the influence of complex factors such as provenance (Garzanti et al. 2021; He et al. 2020), hydrodynamic sorting (Su et al. 2017), chemical weathering related to long-time regional climate (Moon et al. 2007; Shao et al. 2012), seasonal meteorological change (Jian et al. 2020), extreme weather (Deng et al.

Responsible editor: Simon Pulley

✉ Mingkun Li  
limk@m.scnu.edu.cn

✉ Tingping Ouyang  
oyangtp@m.scnu.edu.cn

<sup>1</sup> School of Geography, South China Normal University, Guangzhou 510631, China

<sup>2</sup> Department of Municipal Engineering, Guangdong Polytechnic of Water Resources and Electric Engineering, Guangzhou 510635, China

<sup>3</sup> Guangdong Nonferrous Metals Engineering Investigation Design Institute, Guangzhou 510080, China

2019), and human activities (Zhang et al. 2011; Szczepaniak-Wnuk et al. 2020), most of geochemical and mineralogical properties of river sediments exhibit non-conservative and heterogeneous features in response to seasons and reaches (Garzanti et al. 2010; Koiter et al. 2013; Deng et al. 2019; Garzanti et al. 2021; He et al. 2020; Jian et al. 2020). In order to understand the heterogeneity of river sediments, it is necessary to study the physical and chemical properties of river sediments at different scales.

Magnetic minerals are ubiquitous in soils and sediments on the earth's surface (Pulley et al. 2017; Yang et al. 2020; Warriar et al. 2021). Magnetic parameters of the riverine sediments provide an accessible record of the natural and anthropogenic changes of river basins (Franke et al. 2009) owing to the quick, nondestructive, and cost-efficient magnetic measurements. Soil parent material is considered to be the primary factor in controlling the magnetism of river sediment. For instance, the mafic rocks (e.g., basalt) in the source areas result in a higher concentration of magnetic minerals in rivers than the areas covered by other rocks (Sudarningsih et al. 2017; Panwar et al. 2020). The influence of hydrodynamic sorting on the magnetism of river sediment is typically of secondary importance. The magnetic particles in some river sediments become finer, and the concentration of magnetic minerals decrease in a downstream direction (Li et al. 2017; Mzuza et al. 2017). However, the influence of hydrodynamic sorting on river sediment magnetism has been shown to be complex. For example, the grain sizes of preferential magnetic particles are different in two branches of the Yangtze River (Dong et al. 2014). A comprehensive study of sediment magnetism throughout the basin helps to understand the influence of hydrodynamic sorting on the distribution of magnetic minerals.

In addition to the abovementioned natural factors, anthropogenic factors have been recognized to be highly important

controls on sediment magnetism. Generally, sediment magnetism tends to be elevated due to the human activity for rivers flowing through cities (Szczepaniak-Wnuk et al. 2020), F-smelting plants (Zhang et al. 2011), and other industrial and residential areas (Chaparro et al. 2008, 2011; Mariyanto et al. 2019). Several studies have assessed the degree of human activity or pollution by the increased magnetic susceptibility (Chaparro et al. 2008; Mariyanto et al. 2019); however, some studies reported that the parent rocks (e.g., volcanic material) and specific weathering conditions could also cause dramatic magnetic enhancements (Liu et al. 2017; Shen et al. 2020; Zhang et al. 2020). Further mineralogical studies, such as the observation on the morphology of magnetic particles, could provide more specific evidence for the existence of artificial magnetic particles (e.g., Franke et al. 2009). Notably, most researches focus on magnetic particles produced by modern human activities and their environmental impact (Chaparro et al. 2008, 2011; Mariyanto et al. 2019; Szczepaniak-Wnuk et al. 2020; Zhang et al. 2011), but there is a lack of understanding of whether ancient human activities are still affecting magnetic minerals in rivers. The mining and smelting of iron ore began to flourish about 2000 years ago (Lynch 2003). Therefore, it was speculated that there may be iron residues from ancient smelting in fluvial sediments, which could be discovered by the magnetic approach.

In order to verify this hypothesis, the Liuxi River with ancient mining records was selected for the present study. The Liuxi River flows through the northeastern Guangzhou of China, and has a large drop along its longitudinal profile. The basin is covered with a mixture of granite, metamorphic, and sedimentary rocks. In addition, human activities are concentrated in the lower reaches (Fig. 1). Therefore, the river is a natural laboratory for investigating the changes of magnetic minerals with the drainage environment. The comprehensive effects of natural processes and human activities

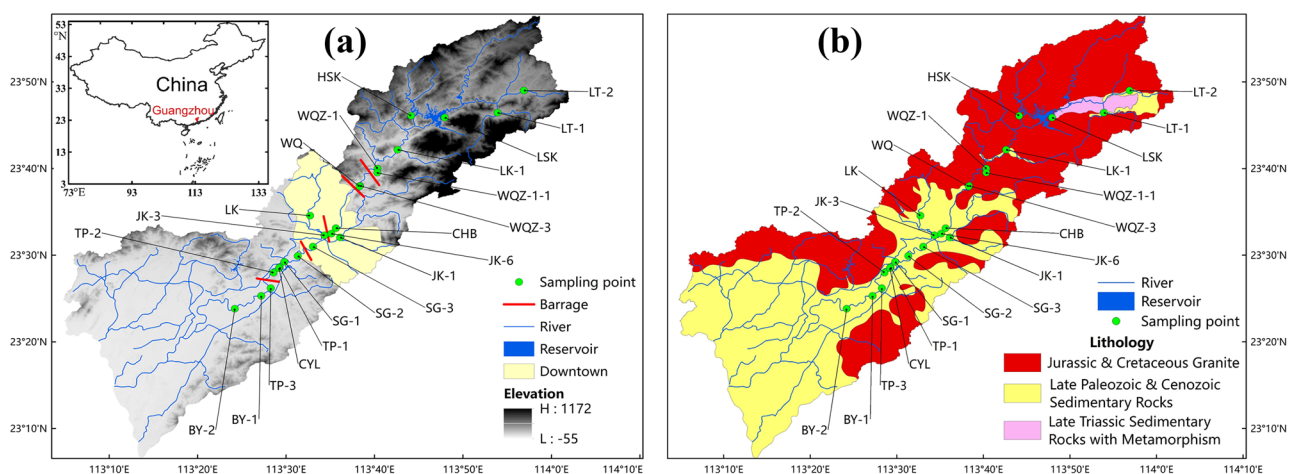


**Fig. 1** a Location of the study area and the river, the downtown, reservoirs, and sampling sites. b The lithology of the study area

on sediment magnetic properties would be discussed based on environmental magnetic parameters, particle sizes, and elemental geochemistry.

## 2 Materials and methods

### 2.1 Study area

Located in the central and northern part of the Pearl River Delta, the Liuxi River is the longest river flowing through Guangzhou, one of the largest cities in southern China (Fig. 1a) (Ji et al. 2013). The Liuxi River has a total length of ~171 km and a total basin area of ~2300 km<sup>2</sup>. The watershed area accounts for 31% of the total land area of Guangzhou, being an important water conservation area. The Liuxi River originates from the Guifeng Mountain in Lutian Town, passes through Conghua and Huadu Districts, and then flows into the Pearl River. In addition to the trunk stream, there are five tributaries with a rainfall collecting area of more than 100 km<sup>2</sup>, including three rivers in the upper reaches and one river respectively in the middle and lower reaches. The basin is located in the subtropical monsoon humid climate zone, crossing the Tropic of Cancer (23° 26' N). The annual average values of temperature, evaporation, and rainfall are 20–22 °C, 1200 mm, and 1800 mm, respectively. Affected by monsoon and typhoons, the rainfall is concentrated during April to September (Huang and Zhao 2017).

The upstream of the Liuxi River is covered by medium-grained porphyry biotite monzogranite, which was formed during the Jurassic and Cretaceous. Notably, in the Late Triassic, sedimentary rocks with remarkable metamorphism emerge which are on the eastern side of the modern day Liuxi Reservoir. Along the metamorphic zone, there are sporadic iron ore deposits formed by the skarnization. The outcrops of the middle and lower reaches of the river are mainly the Late Paleozoic (Devonian to Carboniferous) and Cenozoic (Eocene and Quaternary) sedimentary rocks, including shale, siltstone, fine sandstone, etc. (Fig. 1b).

In the upstream of the Liuxi River, Liangkou and Lutian are the main town centers. Due to the geographical limitations of industrial development, agriculture and ecological tourism are the primary industries present, and building materials and small hydropower are the leading industrial enterprises. The urban and rural settlements are more concentrated in the lower part of the river basin (Li 2020). The downtown along the Liuxi River, centered around Jiekou, Jiangpu, and suburbs (Fig. 1a), mainly provides residential, cultural entertainment, business, and trade functions. The Taiping Town in the lower reaches has an advantageous geographical location and convenient transportation and mainly develops high-tech industries, manufacturing, and other service industries (Huang and Zhao 2017).

### 2.2 Sampling

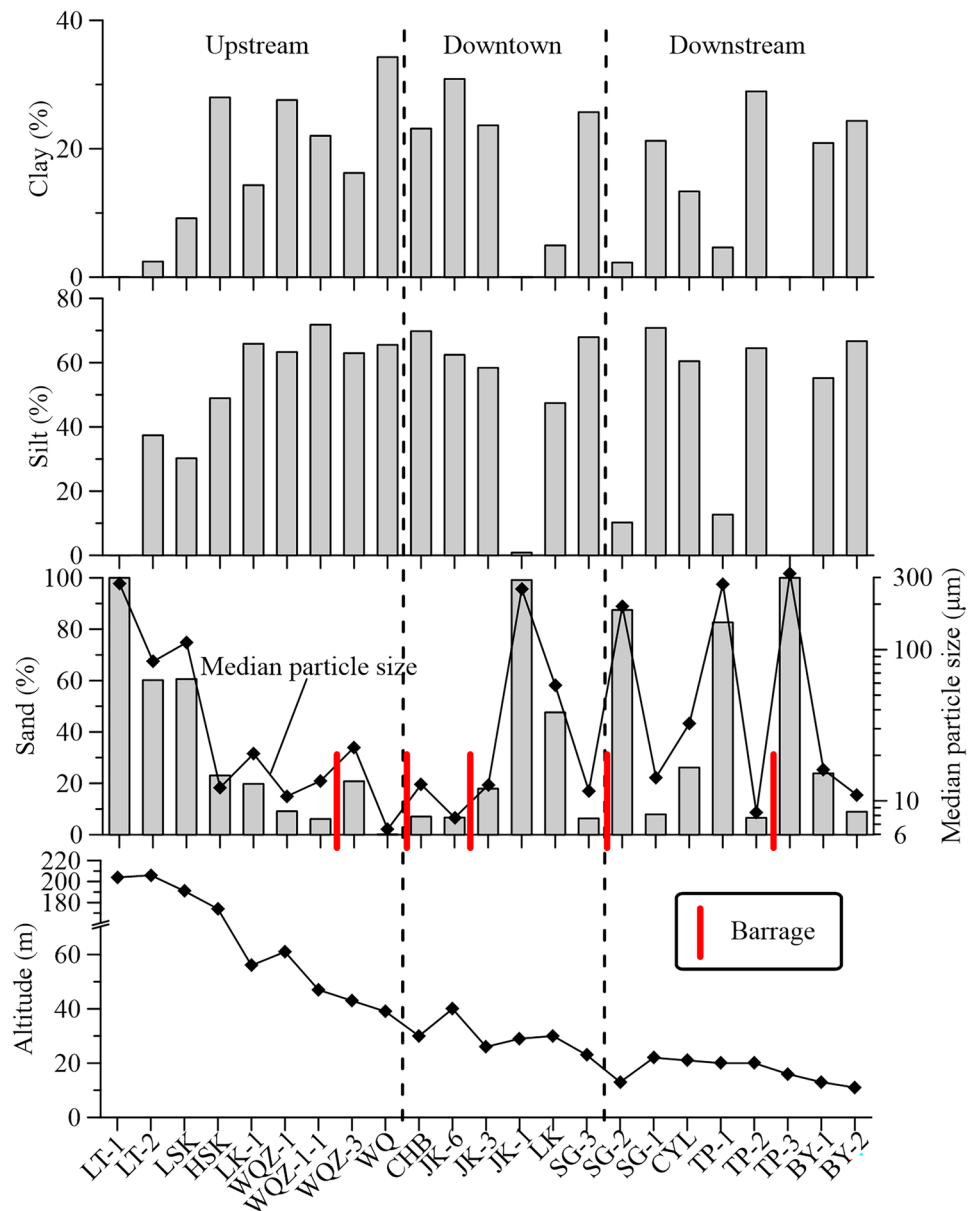
Twenty-three sites were set up in the Liuxi River to collect sediment samples (Fig. 1). A stainless-steel grab was used to collect sediment samples to a depth of approximately 10 cm from the river bed. The environment of the sampling sites was recorded and photographed, and the sediment samples were described. The sampling interval was 3–10 km in the upper reaches, and 2–3 km in the middle (downtown of Conghua District) and lower reaches (villages and towns of Baiyun District). The altitudes of sampling sites range from 200 to 10 m above sea level from upstream to downstream of the Liuxi River (Fig. 2). In addition, three iron ore samples (TK-1, TK-2, and TK-3) were collected on the upper mountain slope of LT-1.

### 2.3 Magnetic measurements

All samples were air dried and packed in 2 × 2 × 2 cm<sup>3</sup> cubic boxes for magnetic measurement. Low- ( $\chi_{lf}$ ) and high-frequency susceptibilities ( $\chi_{hf}$ ) were measured using a Kappabridge MFK1-FA and normalized by sample mass (Liu et al. 2017; Shen et al. 2020; Szczepaniak-Wnuk et al. 2020; Li et al. 2021). The  $\chi_{lf}$  was also measured for the three iron ore samples. Low-frequency susceptibilities ( $\chi_{lf}$ ) is an indicator of the total magnetic mineral concentration, including low-coercivity magnetic/ferrimagnetic minerals (e.g., magnetite, maghemite), high-coercivity magnetic/antiferromagnetic minerals (e.g., hematite, goethite), with different magnetic domains (superparamagnetic (SP) domain, single domain (SD), “pseudo-single domain”, and multidomain). The formula  $\chi_{fd}(\%) = 100 \times (\chi_{lf} - \chi_{hf}) / \chi_{lf}$  was applied to calculate the parameter  $\chi_{fd}(\%)$  (Oldfield et al. 1983), which was used to express the contribution of ultrafine-grained particles (e.g., SP to SD particles) to the total  $\chi_{lf}$ .

Then, after applying the corresponding magnetic field, the anhysteretic remanence (ARM), saturated isothermal remanence ( $SIRM = IRM_{2000\text{ mT}}$ ), and the isothermal remanence ( $IRM_{-100\text{ mT}}$ ,  $IRM_{-300\text{ mT}}$ ) were measured successively by using a JR-6 magnetometer. Saturated isothermal remanence magnetization (SIRM) represents concentration of remanence-carrying magnetic minerals, but has no relation with the SP grains.  $S_{-100} = -IRM_{-100\text{ mT}} / SIRM$  and  $S_{-300} = -IRM_{-300\text{ mT}} / SIRM$  were used to calculate  $S_{-100}$  and  $S_{-300}$ . The larger the parameters are, the higher the relative content of magnetic minerals with low coercivity (such as magnetite). The HIRM, calculation formula  $HIRM = (IRM_{-300\text{ mT}} + SIRM) / 2$ , was used to reflect the content of high-coercivity magnetic minerals (such as hematite and goethite) (Bloemendal et al. 1988).  $\chi_{ARM}$  was obtained from the ratio of ARM to the direct current (DC) magnetic field, and is sensitive to the single domain (SD) particles (relatively fine particles). Therefore,  $\chi_{ARM} / \chi_{lf}$  can be used to reflect the

**Fig. 2** Spatial variations of clay, silt, sand, and the median particle size



size of magnetic particles. The larger value corresponds to a fine particle size.

In order to understand the hysteresis characteristics of samples, the LakeShore 8604 vibrating sample magnetometer (VSM) was used to measure the hysteresis loop, isothermal remanence (IRM) acquisition curve, and reverse demagnetization curve for all sediment samples, and the TK-1 and TK-2. According to the hysteresis loops and IRM acquisition curves, three types were discovered, and three samples (LT-1, BY-2, and TP-2) from the three types was selected for the first-order reversed curve (FORC) test. The FORC diagram is useful in describing the hysteresis characteristics and identifying the origin of magnetic minerals (Roberts et al. 2000, 2018). The

measured methods were described by Li et al. (2021). All the magnetic measurements were conducted in the Laboratory of Environmental Magnetism of South China Normal University.

## 2.4 Observations of magnetic minerals

Magnets were used to extract the magnetic particles from the samples of LT-1, WQ, and SG-1. Then, a scanning electron microscope (SEM) was used to observe the micromorphology of particles, and an energy dispersive spectrometer (EDS) was used to analyze their elemental composition. The sample extraction and testing procedure followed the methods of Li et al. (2021).

## 2.5 Particle size measurements

Each sample of less than 1 g was placed into a 50-mL beaker, and approximately 10 mL of 1 mol/L dilute hydrochloric acid (HCl) was added. Each beaker was placed in a water bath (80 °C) for 2 h to ensure that the sample reacted sufficiently with HCl to remove any carbonates present. Then, about 5 mL of 30% hydrogen peroxide (H<sub>2</sub>O<sub>2</sub>) was added. The solution was heated for 2 h to remove sediment-associated organic matter and disperse soil aggregates. After the reaction was completed when there were no bubbles, the solution was repeatedly washed using deionized water until a neutral pH was reached. Before the sample test, 10 mL of 0.5 mol/L sodium hexametaphosphate was added, and then the solution was placed in an ultrasonic vibrator for 10 min. Each sample was measured three times with a laser particle size analyzer Malvern 3000, and the average values of median particle grain size (Md), sand, silt, and clay were taken as the final test result.

## 2.6 Geochemical measurements

After each sample was dried at room temperature, it was ground to pass a 200-mesh sieve (74 μm). Elements, including Al, Fe, K, Mg, Ca, Na, Si, Ba, Ca, Ni, P, Pb, Sn, S, Sr, Ti, V, Zr, As, Cl, Co, Cr, Cu, Bi, Mo, Sb, and W, were tested by an X-ray fluorescence (XRF) spectrometer. After the samples were dried at 105 °C, each sample was accurately weighed, and placed in a platinum crucible. The mixed flux of lithium tetraborate–lithium metaborate–lithium nitrate was added to confirm that the sample and the flux were completely mixed. The high-precision melting sample machine was then applied to melt the sample at 1050 °C. After that, the molten slurry was poured into a platinum mold to form a frit after cooling. The fused piece was checked to confirm the quality (if the fused piece was unqualified, the sample must be reweighed and melted), and then the main quantity was measured with an XRF spectrometer. To ensure the accuracy of the test, a relatively large platinum mold was used. Meanwhile, another dried sample was accurately weighed and burned in an aerobic muffle furnace at 1000 °C, and then accurately weighed after cooling. The weight difference before and after combustion was the loss on ignition (LOI).

In order to estimate the degree of sediment weathering, two most commonly used chemical weathering parameters, including chemical index of alteration [ $CIA = 100 (Al_2O_3 / (Al_2O_3 + (CaO - 3.33P_2O_5 + Na_2O + K_2O)))$ ] (Nesbitt and Young 1982) and weathering index [ $WIP = 100 ((CaO - 3.33 \cdot P_2O_5) / 0.7 + 2Na_2O / 0.35 + 2K_2O / 0.25 + MgO / 0.9)$ ] (Parker 1970), were calculated using molecular proportions of mobile alkali and alkaline earth metals corrected for Ca in apatite (Garzanti et al. 2013).

## 3 Results

### 3.1 Particle size features

The studied samples are composed of sand, clayey silt, and silty sand (Shepard 1954). The average sand content in the upstream (LT-1 to WQ), downtown (CHB to SG-3), and downstream (SG-2 to BY-2) samples are 37.45%, 29.76%, and 38.89%, respectively (Fig. 2). The average silt contents of the upstream, downtown, and downstream samples are 47.57%, 50.75%, and 45.40%, respectively. The average clay content in the upstream, downtown, and downstream samples are 14.97%, 19.48%, and 15.71%, respectively. In general, silty sediments account for most of the total content, and the contents of the sand and clay are variable.

The median particle size (Md) of all samples ranges from 6 to 318 μm, indicating a wide range of particle size. Notably, the Md of sites locating in downstream of the barrage (WQZ-3, CHB, JK-1, SG-2, and TP-3) is coarser than other sites nearby (Fig. 2). Except for the abnormally high values (193–318 μm) for Sites JK-1, SG-2, TP-1, and TP-3 in the lower reach, the Md tends to be roughly finer downstream.

### 3.2 Magnetic properties

#### 3.2.1 Spatial distributions of magnetic parameters

In terms of magnetic concentrations, the site LT-1 contains the highest magnetic contents due to the highest values of  $\chi_{lf}$  ( $8610 \times 10^{-8} \text{ m}^3 \cdot \text{kg}^{-1}$ ), SIRM ( $822 \times 10^{-3} \text{ Am}^2 \cdot \text{kg}^{-1}$ ), HIRM ( $36,941 \times 10^{-6} \text{ Am}^2 \cdot \text{kg}^{-1}$ ), and  $\chi_{ARM}$  ( $5713 \times 10^{-8} \text{ m}^3 \cdot \text{kg}^{-1}$ ) (Fig. 3a–d). These values are tens to hundreds of times higher than the average values of other sediment samples. In contrast, the three iron ore samples have the  $\chi_{lf}$  values of  $21,342$ – $38,845 \times 10^{-8} \text{ m}^3 \cdot \text{kg}^{-1}$ , which are 2.5–4.5 times of the LT-1. The average values of  $\chi_{lf}$  in the upstream (except LT-1), downtown, and downstream samples are  $41.76 \times 10^{-8} \text{ m}^3 \cdot \text{kg}^{-1}$ ,  $42.38 \times 10^{-8} \text{ m}^3 \cdot \text{kg}^{-1}$ , and  $22.37 \times 10^{-8} \text{ m}^3 \cdot \text{kg}^{-1}$ , respectively (Fig. 3a). The average values of SIRM in the upstream (except LT-1), downtown, and downstream samples are  $4.03 \times 10^{-3} \text{ Am}^2 \cdot \text{kg}^{-1}$ ,  $4.13 \times 10^{-3} \text{ Am}^2 \cdot \text{kg}^{-1}$ , and  $1.92 \times 10^{-3} \text{ Am}^2 \cdot \text{kg}^{-1}$ , respectively (Fig. 3b). The HIRM average in the upstream (except LT-1), downtown, and downstream samples are  $323 \times 10^{-6} \text{ Am}^2 \cdot \text{kg}^{-1}$ ,  $288 \times 10^{-6} \text{ Am}^2 \cdot \text{kg}^{-1}$ , and  $233 \times 10^{-6} \text{ Am}^2 \cdot \text{kg}^{-1}$ , respectively, indicating that the high-coercivity magnetic minerals (e.g., hematite and goethite) gradually decrease from the upstream to the downstream of the Liuxi River (Fig. 3c). The average  $\chi_{ARM}$  in the upstream, downtown, and downstream samples are  $64.01 \times 10^{-8} \text{ m}^3 \cdot \text{kg}^{-1}$ ,

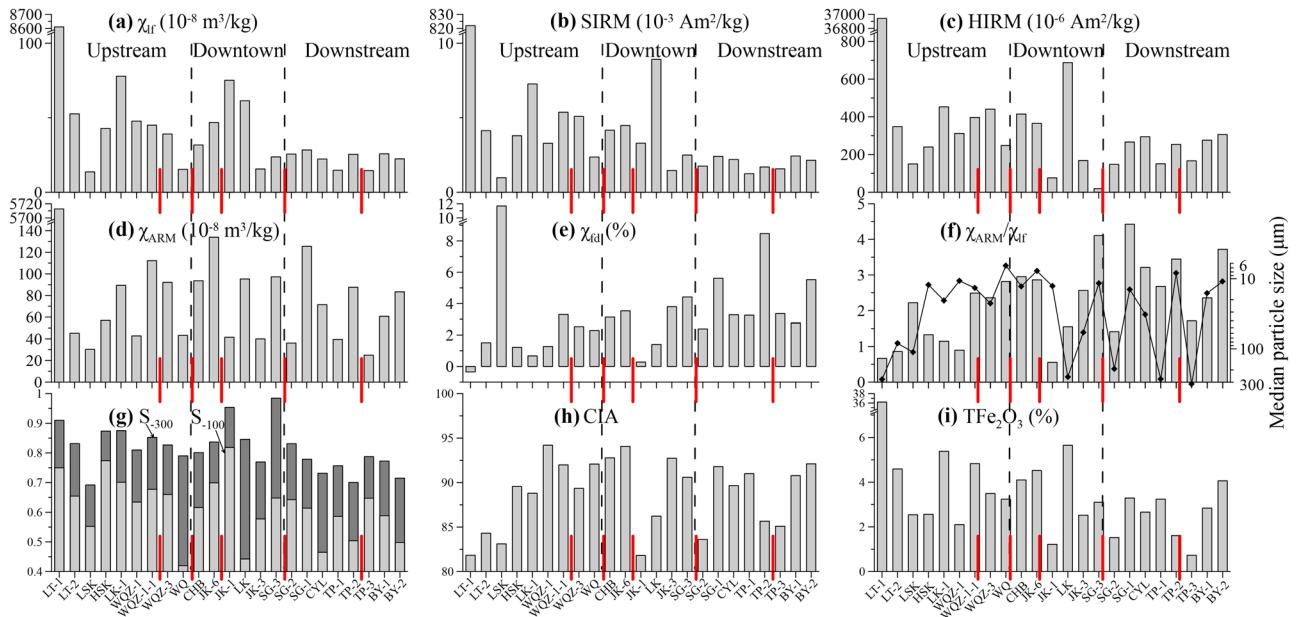


**Fig. 3** Spatial distributions of **a**  $\chi_{If}$ , **b** SIRM, **c** HIRM, **d**  $\chi_{ARM}$ , **e**  $\chi_{fd}$ , **f**  $\chi_{ARM}/\chi_{If}$  and median particle size, **g**  $S_{300}$  and  $S_{100}$ , **h** CIA, and **i**  $TFe_2O_3$

$83.58 \times 10^{-8} \text{ m}^3 \cdot \text{kg}^{-1}$ , and  $66.14 \times 10^{-8} \text{ m}^3 \cdot \text{kg}^{-1}$ , respectively. Overall, the magnetic concentrations show a decline tendency in the downstream, owing to the spatial distributions of  $\chi_{If}$ , SIRM, and HIRM (Fig. 3a–c), while  $\chi_{ARM}$  shows a more discrete than previous parameters (Fig. 3d). In addition, the  $\chi_{If}$  values at Sites CHB, JK-3, and SG-2 increase compared with the previous site, indicating that the magnetic concentrations increase after flowing through the barrage (Fig. 3a). Except for the values of LT-1, the mean values of  $\chi_{If}$  and SIRM of all samples increase in the downtown, and the coefficient of variance (CV) all exceed 20% in the entire river, indicating that the magnetic contents in the downtown increase due to highly variable distribution in the Liuxi River.

Regarding the magnetic grain size, LT-1 has the coarsest magnetic minerals without significant quantities of fine SP grains, which is derived from the lowest  $\chi_{ARM}/\chi_{If}$  (0.66) and  $\chi_{fd}$  (−0.35%). Apart from LT-1, the  $\chi_{fd}$  average in the upstream, downtown, and downstream samples are 3.06%, 2.43%, and 4.34%, respectively, which means the contributions of SP and stable SD particles to the magnetic susceptibility increased in the downstream of the Liuxi River (Fig. 3e). Therefore, based on the highest  $\chi_{ARM}$ , the fine SD magnetic grains in the downtown are relatively abundant compared with the upstream and downstream. The  $\chi_{ARM}/\chi_{If}$  average increases from 1.76 upstream to 2.87 downstream, indicating that the refining of magnetic minerals from upstream to downstream (Fig. 3f). Obviously, the magnetic mineralogy of sites located downstream of the barrage (WQZ-3, JK-3, SG-2, and TP-3) is coarser than other sites

nearby due to their relatively low  $\chi_{ARM}/\chi_{If}$ . It is also worth noting that the CV of the parameters ( $\chi_{fd}$ ,  $\chi_{ARM}$ ,  $\chi_{ARM}/\chi_{If}$ ) for evaluating the magnetic particle size is all greater than 30% in the Liuxi River.

The average values of  $S_{300}$  in the upstream (including LT-1), downtown, and downstream samples are 0.83, 0.86, and 0.76, respectively. The sediments in the river downstream have the relatively low values of  $S_{100}$  and  $S_{300}$ , although the values of the entire river system are variable (Fig. 3g). Deduced from the  $S_{300} > 0.7$  in all samples, it could infer that the Liuxi River samples, especially in the downtown, are dominated by ferrimagnetic minerals with partial interfusion of high-coercivity magnetic minerals (e.g., hematite and goethite) (Fig. 3g).

### 3.2.2 Hysteresis characteristics of magnetic minerals

The hysteresis loops of all samples can be divided into three categories (Fig. 4a–e). The hysteresis loop of LT-1 after paramagnetic slope correction overlaps with the original hysteresis loop, and the magnetization reaches saturation at about 100 mT (Fig. 4a). This feature is consistent with the iron ore samples, TK-1 and TK-2 (Fig. 4b, c). The other two types are similar, while the saturation magnetization fields are different (Fig. 4d, e). The saturation magnetization field of most samples, such as the WQ (Fig. 1d), is below 800 mT, and the coercivity ( $B_c$ ) is less than 100 mT. Different with those samples, the magnetization of TP-2 does not reach saturation when the magnetic field intensity reaches 800 mT (Fig. 4e). The IRM of TP-2 reaches 80% of the saturation

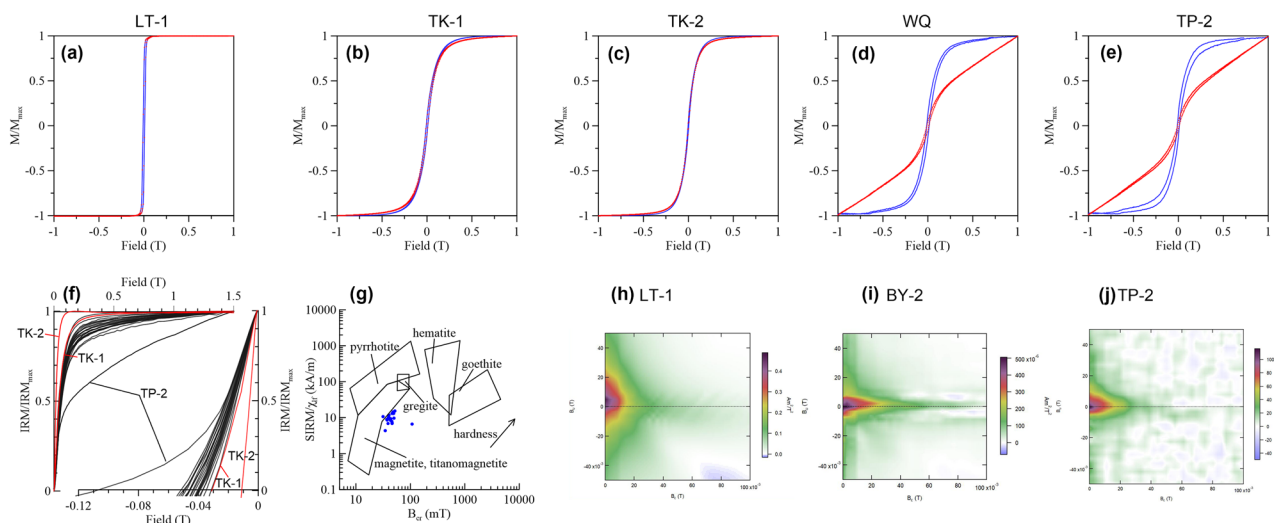


**Fig. 4** Hysteresis loops of **a** LT-1, **b** TK-1, **c** TK-2, **d** WQ, and **e** TP-2. Red and blue curves are normalized to the  $M_s$  values at 1 T before and after paramagnetic slope correction (corrected from the slope above 70% of the maximum applied field where the mag-

netization is saturated), respectively. **f** IRM acquisition curves and back-field curves for all samples, **g**  $SIRM/\chi_{if}$  vs.  $B_{cr}$  plot (Peters and Thompson 1998). FORC diagrams of **h** LT-1, **i** BY-2, and **j** TP-2

value at about 750 mT, while the remanence coercivity ( $B_{cr}$ ) is about 107 mT (Fig. 4f). In contrast, other samples reach 80% of the IRM saturation value at about 100~230 mT, and the  $B_{cr}$  is concentrated at 30~50 mT (Fig. 4f). All samples are plotted in the area close to (titano) magnetite, with a hardness trend due to the addition of the “hard” magnetic component (e.g., hematite and goethite) (Fig. 4g) (Peters and Thompson 1998). Therefore, the iron oxides/hydroxides are dominant in the magnetic minerals.

The FORC diagram is quite sensitive in identifying the state of magnetic domains (Pike et al. 1999; Roberts et al. 2000, 2015). All the contour lines of three measured samples have large vertical distributions at  $B_c = 0$ . The vertical distribution of LT-1 is greater than 30 mT and relatively flat (Fig. 4h). However, the vertical distribution of TP-2 is steeper with a range of about 10 mT due to its narrow horizontal distribution, suggesting a low coercive force distribution is lower (Fig. 4j). Generally, the detrital magnetites could be identified by the FORC diagrams, because most of them are MD and “pseudo-single domain” (“PSD”, or “vortex”) that could be characterized by the maximum values at  $B_c < 20$  mT, and a large vertical distribution at  $B_c = 0$  (Roberts et al. 2018). In contrast, the FORC diagram of bacterial magnetosomes has a typical weak magnetic interaction SD particle behavior, and its distribution is horizontally extended. Obviously, the lack of this type of FORC diagram could determine that magnetite mineral is produced from debris in all samples, instead of magnetotactic bacteria (Roberts et al. 2018).

In summary, it can be roughly inferred that most of the samples were dominated by the detrital magnetite and a

small amount of high-coercivity minerals (e.g., hematite). The MD ferrimagnetic minerals predominate the LT-1 sample without paramagnetic and SP particles.

### 3.2.3 SEM and EDS results

It can be observed from the SEM images that most magnetic particles of the LT-1 have obvious edges and corners with a large particle size (about 40  $\mu\text{m}$ ) accompanied by cracks. Meanwhile, the EDS results of two sites indicate that the count of Fe in magnetic particles is extremely high, while the count of Al is very low (Fig. 5a). The SG-1 located in the lower reach of the river contains magnetic spherules with a diameter of 10  $\mu\text{m}$ , and metal elements of Mg, Ti, Zn, K, and Cr are detected (Fig. 5b). In addition, particles with layers and corners exist in SG-1 (Fig. 5b). The spherical magnetic particles with large enrichment of Fe and angular particles with sharp or round ridges are found in the CHB located in the downtown (Fig. 5c). The composition of CHB particles seems to be similar with SG-1; however, the particle size of CHB (about 25  $\mu\text{m}$ ) is larger than that of SG-1 (Fig. 5c).

### 3.3 Elemental geochemistry

Different from other samples,  $\text{Fe}_2\text{O}_3$  content of LT-1 reaches up to 36.21%, about 11.42 times higher than the  $\text{Fe}_2\text{O}_3$  average for other samples, even reaching the grade of lean ore (Luo 2005). The LT-1 contains the highest contents of some of the main elements, including  $\text{Fe}_2\text{O}_3$ , MnO, CaO, and the metals, including NiO, PbO,  $\text{SnO}_2$ ,  $\text{V}_2\text{O}_5$ , ZnO,  $\text{As}_2\text{O}_3$ , CoO,  $\text{Cr}_2\text{O}_3$ , CuO, Bi, Mo, and W (Table 1). For the

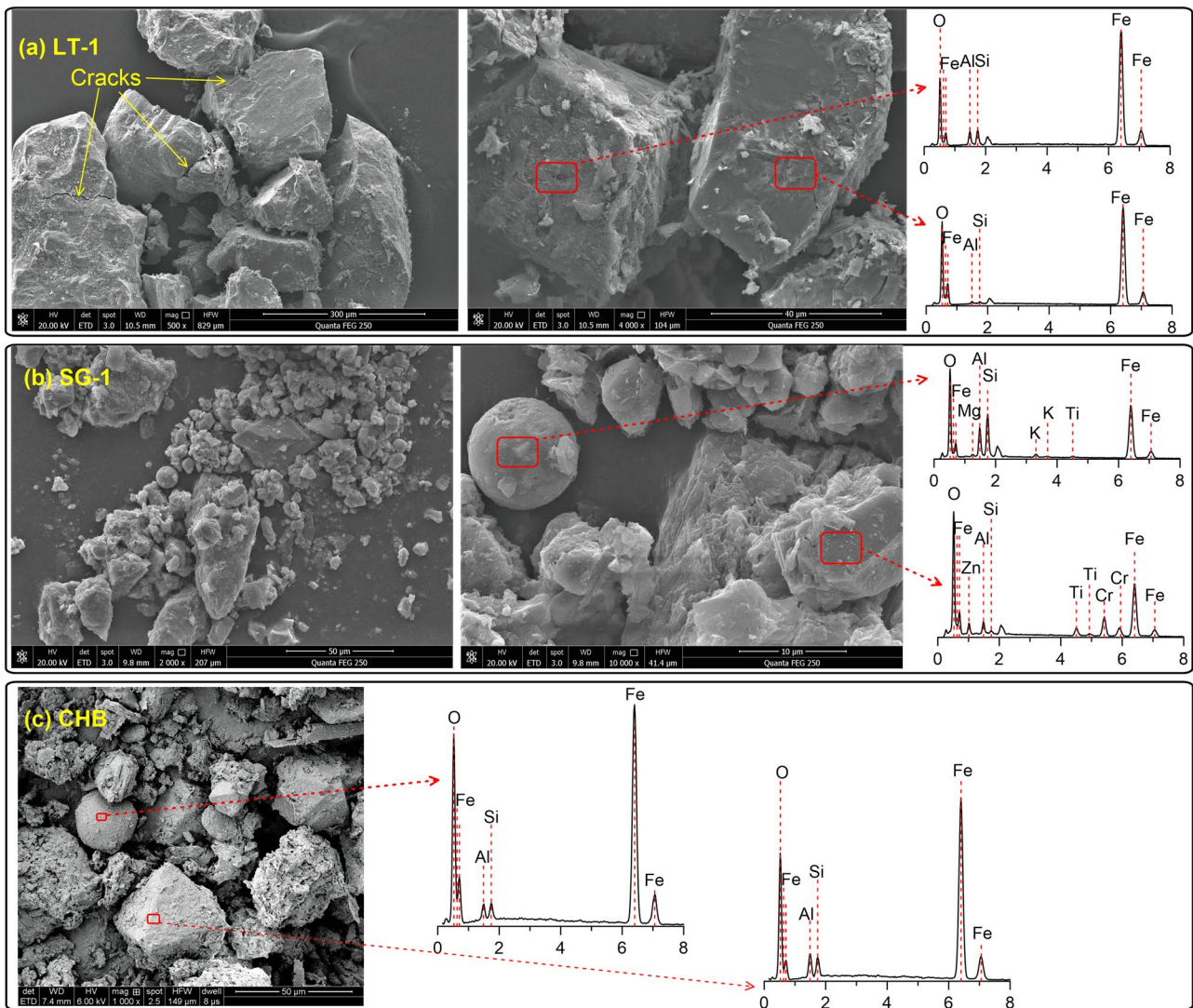


**Fig. 5** SEM and EDS results for **a** LT-1, **b** SG-1, and **c** CHB

other samples, most of metal elements cannot be accurately detected by the XRF method due to their low contents in the samples. Besides, the LT-1 contains the lowest contents of  $\text{Al}_2\text{O}_3$ ,  $\text{K}_2\text{O}$ ,  $\text{Na}_2\text{O}$ , and  $\text{SiO}_2$ . Except for LT-1, the content of  $\text{Fe}_2\text{O}_3$  average reduces from 3.59% in the upstream to 2.49% in the downstream (Fig. 3i). The average values of CIA in the upstream (including LT-1), downtown, and downstream samples are 88.36, 89.71, and 88.71, respectively, suggesting a slight difference in the degree of chemical weathering throughout the river (Fig. 3h). The sites located downstream of the barrage (WQZ-3, JK-3, SG-2, and TP-3) have lower degree of chemical weathering, which is inferred from its relatively low CIA (Fig. 3h).

Compared with the standard of Upper Continental Crust (UCC), the results show the enrichment of  $\text{SiO}_2$  and  $\text{K}_2\text{O}$ , as well as the loss of  $\text{Na}_2\text{O}$ ,  $\text{CaO}$ ,  $\text{MgO}$ , and  $\text{Fe}_2\text{O}_3$  (Taylor

and McLennan 1985) (Fig. 6). In addition, the total content of  $\text{Al}_2\text{O}_3$ ,  $\text{TiO}_2$ ,  $\text{MnO}$ , and  $\text{P}_2\text{O}_5$  are close to UCC, and those of  $\text{Al}_2\text{O}_3$  and  $\text{TiO}_2$  greatly vary at different sites. The  $\text{Fe}_2\text{O}_3/\text{UCC}$  of LT-1 reaches 7, indicating that the magneto tactic  $\text{Fe}_2\text{O}_3$  content in LT-1 is extremely high. The almost-lowest content of  $\text{SiO}_2$  and the highest MnO at LT-1 also confirm the previous results.

## 4 Discussion

### 4.1 Reasons for the extremely high magnetic content in LT-1

The magnetic minerals of the sample LT-1 are mainly MD magnetite without SP particles, and the content of magnetic



**Table 1** Element results of the surface sediments in the Liuxi River

Elements/oxides	Al <sub>2</sub> O <sub>3</sub>	Fe <sub>2</sub> O <sub>3</sub>	K <sub>2</sub> O	MgO	MnO	Na <sub>2</sub> O	SiO <sub>2</sub>	BaO	CaO	NiO	P <sub>2</sub> O <sub>5</sub>	PbO	SnO <sub>2</sub>	SO <sub>3</sub>	LOI	SrO	TiO <sub>2</sub>	V <sub>2</sub> O <sub>5</sub>	ZnO	ZrO <sub>2</sub>	As <sub>2</sub> O <sub>3</sub>	Cl	CoO	Cr <sub>2</sub> O <sub>3</sub>	CuO	Bi	Mo	Sb	W
Unit	%	%	%	%	%	%	%	%	%	%	%	%	%	%	%	%	%	%	%	%	%	%	%	%	%	µg g <sup>-1</sup>	µg g <sup>-1</sup>	µg g <sup>-1</sup>	µg g <sup>-1</sup>
Limit of detection	0.01	0.01	0.01	0.01	0.01	0.01	0.01	0.01	0.01	0.01	0.01	0.01	0.01	0.01	0.01	0.01	0.01	0.01	0.01	0.01	0.01	0.01	0.01	0.01	0.01	2	1	5	10
Upstream	LT-1	5.29	36.21	1.65	0.32	0.24	0.31	53.2	0.03	1.1	0.02	0.07	0.02	0.24	0.07	0.01	0.27	0.27	0.07	0.04	0.03	0.01	0.01	0.01	0.02	148	8	<5	230
	LT-2	13.94	4.59	5.08	0.64	0.07	0.54	69.4	0.09	0.63	0.01	0.07	<0.01	0.01	0.03	0.01	0.71	0.71	0.02	0.05	<0.01	<0.01	<0.01	0.02	<0.01	2	1	<5	<10
	LSK	16.44	2.54	6.76	0.25	0.05	0.26	67.7	0.05	0.81	0.01	0.03	0.01	0.01	0.11	0.01	0.28	0.28	0.01	0.03	<0.01	<0.01	<0.01	0.01	<0.01	<2	1	<5	<10
	HSK	14.19	2.56	3.62	0.12	0.03	0.15	73.7	0.02	0.08	0.01	0.02	0.02	0.01	0.03	0.01	0.37	0.37	0.01	0.07	<0.01	<0.01	<0.01	0.01	<0.01	<2	4	<5	10
	LK-1	14.88	5.38	3.74	0.43	0.06	0.54	68.7	0.04	0.29	0.01	0.07	0.01	0.01	0.12	0.01	0.47	0.47	0.01	0.07	<0.01	<0.01	<0.01	0.01	<0.01	2	6	<5	10
	WQZ-1	13.4	2.1	1.66	0.09	0.02	0.23	75.9	0.01	0.08	0.01	0.02	<0.01	0.01	0.03	<0.01	0.25	0.25	<0.01	0.02	<0.01	<0.01	<0.01	0.01	<0.01	<2	4	<5	<10
	WQZ-1-1	23.58	4.83	4.1	0.48	0.1	0.59	55.7	0.04	0.39	0.02	0.1	0.01	0.01	0.08	0.01	0.51	0.51	0.02	0.04	<0.01	<0.01	<0.01	0.02	<0.01	3	3	<5	10
	WQZ-3	19.36	3.49	4.69	0.34	0.06	0.62	63.9	0.04	0.24	0.01	0.07	0.01	0.01	0.08	0.01	0.48	0.48	0.01	0.06	<0.01	<0.01	<0.01	0.02	<0.01	<2	3	<5	10
Downtown	WQ	18.63	3.24	3.33	0.29	0.05	0.41	64.8	0.03	0.24	0.01	0.09	<0.01	0.01	0.1	0.01	0.37	0.37	0.01	0.02	<0.01	<0.01	<0.01	0.01	<0.01	<2	3	<5	10
	CHB	17.88	4.1	2.98	0.33	0.08	0.38	64.7	0.03	0.29	<0.01	0.14	<0.01	0.01	0.13	0.01	0.46	0.46	0.02	0.03	<0.01	<0.01	<0.01	0.01	<0.01	2	3	<5	10
	JK-6	22.59	4.52	3.41	0.38	0.09	0.4	54.6	0.04	0.35	<0.01	0.29	<0.01	0.01	0.28	0.01	0.5	0.5	0.02	0.04	<0.01	<0.01	<0.01	0.01	<0.01	3	4	<5	10
	JK-1	7.03	1.22	2.92	0.11	0.02	0.52	86.9	0.06	0.3	<0.01	0.03	<0.01	0.01	0.02	0.01	0.25	0.25	<0.01	0.04	<0.01	<0.01	<0.01	0.01	<0.01	<2	1	<5	<10
	LK	12.94	5.65	3.55	0.79	0.24	1.07	70.6	0.05	0.76	<0.01	0.16	<0.01	0.01	0.03	0.01	0.9	0.9	0.01	0.03	<0.01	<0.01	<0.01	0.01	<0.01	2	4	5	10
	JK-3	13.6	2.52	2.46	0.14	0.03	0.22	73.8	0.02	0.13	0.02	0.12	<0.01	0.01	0.06	<0.01	0.43	0.43	0.01	0.03	<0.01	<0.01	<0.01	0.02	<0.01	<2	2	<5	10
	SG-3	16.14	3.1	3.67	0.27	0.05	0.4	69	0.03	0.22	<0.01	0.14	0.01	0.01	0.16	0.01	0.51	0.51	0.02	0.05	0.01	<0.01	<0.01	0.01	<0.01	<2	4	6	10
	SG-2	8.69	1.52	3.53	0.13	0.04	0.42	81.6	0.03	0.17	0.02	0.06	<0.01	0.01	0.02	0.01	0.43	0.43	0.01	0.07	0.01	<0.01	<0.01	0.02	<0.01	<2	1	<5	10
	SG-1	14.5	3.29	2.86	0.34	0.06	0.32	71.6	0.03	0.21	0.02	0.13	<0.01	0.01	0.09	0.01	0.55	0.55	0.01	0.06	0.01	<0.01	<0.01	0.03	<0.01	<2	1	<5	10
	CYL	13.38	2.66	3.4	0.3	0.05	0.36	73.9	0.03	0.22	0.02	0.14	0.01	0.01	0.07	0.01	0.45	0.45	0.01	0.06	<0.01	<0.01	<0.01	0.03	0.01	<2	1	<5	10
	TP-1	12.68	3.24	2.66	0.27	0.05	0.24	75.5	0.02	0.24	0.02	0.08	<0.01	0.01	0.03	0.01	0.48	0.48	0.01	0.04	0.01	<0.01	<0.01	0.03	<0.01	<2	2	<5	10
	TP-2	8.8	1.61	3.11	0.16	0.03	0.35	83	0.02	0.12	0.01	0.06	<0.01	0.01	0.06	0.01	0.31	0.31	0.01	0.03	0.01	<0.01	<0.01	0.01	<0.01	<2	1	<5	<10
	TP-3	3.22	0.73	1.14	0.08	0.01	0.19	93.7	0.01	0.07	<0.01	0.03	<0.01	0.01	0.03	<0.01	0.15	0.15	0.01	0.02	<0.01	<0.01	<0.01	0.01	<0.01	<2	<1	<5	<10
	BY-1	13.16	2.84	3	0.29	0.05	0.31	73	0.02	0.26	<0.01	0.16	<0.01	0.01	0.07	0.01	0.46	0.46	0.02	0.05	0.01	<0.01	<0.01	0.01	<0.01	<2	2	<5	10
	BY-2	18.66	4.06	3.42	0.41	0.07	0.37	64.3	0.03	0.27	<0.01	0.12	<0.01	0.01	0.05	0.01	0.65	0.65	0.01	0.06	0.01	<0.01	<0.01	0.01	<0.01	<2	2	<5	10

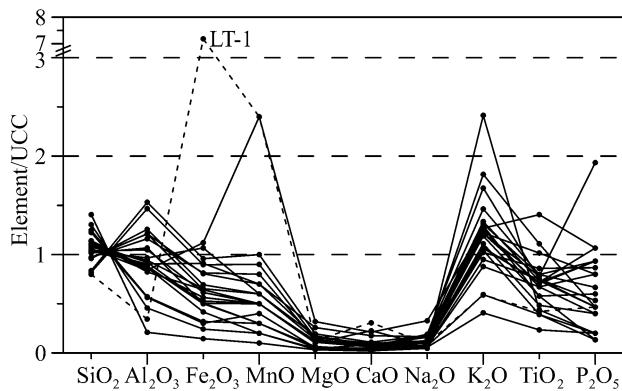


**Fig. 6** UCC-normalized major elements for all the measured samples

minerals is extremely high. Strangely, LT-1 does not contain any paramagnetic components which normally present in silicate minerals (e.g., feldspar and clay minerals) (Zhang et al. 2018). For river sediments, the silicate minerals are derived from the parent rocks or produced during the chemical weathering. It can be deduced that the silicate minerals are not included in the parent rocks of LT-1, and the sample has experienced relatively weak chemical weathering compared with other samples.

The anomalism of LT-1 could be interpreted by the possibility of mixing with the volcanic ash. The  $\chi_{lf}$  value of LT-1 is close to the volcanic ash embedded in a basalt soil profile in Hainan Island, southern China (Liu et al. 2017). However, volcanic ash usually contains abundant SP particles (Liu et al. 2017; Shen et al. 2020). Moreover, there is no document recording the presence of volcanic eruptions nearby; thus, the possibility could be excluded.

Another possibility is that the sample comes from industrial magnetic materials, which do not contain paramagnetic components. The technogenic magnetic particles produced by modern industrial activities such as coal combustion could increase the magnetic concentration (Horng et al. 2009; Lu et al. 2016). However, the observed magnetic particles of LT-1 are all detrital magnetic minerals characterized by cubic and subangular shapes (Fig. 5a). LT-1 is located close to a mountain and a small village without any factories. Thus, the magnetic minerals in LT-1 are unlikely coming from industrial activities.

Historical mining in history could be responsible for the highest magnetic content of LT-1. During the Ming and Qing Dynasties (over the past ~600–100 years), the mining and smelting of iron ore in Lutian prevailed and flourished, and the mined ore was transported to the Pearl River through the Liuxi River (Li 1979; Luo 2005). The mining sites documented by the local chorography (*Fangzhi*) are close to LT-1 with 3–10 km (Fig. 7a–b), although all of the local knowledge for 100 mining sites has not been determined so far

(Luo 2005). During our recent field trip, extensive iron ore and slag were found widespread on the road along the mountain river, upstream of the site LT-1 (Fig. 7c–d). The remains of ancient iron ore/slag could be transported into the river (Fig. 7b). It can be inferred that the magnetite in this sample comes from the direct denudation of rocks by ancient mining activities. According to the regional geological data, the iron ore is a product of skarnization and contains associated metals such as Bi and W (Luo 2005). Therefore, the contents of metal elements are also relatively high in the LT-1. The LT-1 magnetic particles have notably sharp edges and cracks (Fig. 5), which are produced during the rapid denudation of minerals. Only one site with high content of metals was found in this study. In the future, it is necessary to strengthen the researches on the impact of ancient iron ore mining and its associated metals on the modern environment risks.

#### 4.2 Influences of parent rocks on the river sediment magnetism

In general, there are significant differences in the sediment magnetism in different parent rock areas. The upstream shows that the content of magnetic minerals along the river is relatively high, especially between HSK to WQZ-3. The upstream mainly flows through the area covered by the Late Jurassic granite (Fig. 1b). According to the regional geology, the granite is characterized by high content of heavy minerals, in particular, magnetite which accounts for 0.12% of the total weight of the granite. The accessory minerals of the granite contain above 63% of magnetite (Guangdong Geological Survey 2000). The middle and lower reaches of the Liuxi River are dominated by Devonian to Quaternary sedimentary rocks, primarily calcareous mudstone, calcareous shale, and siltstone. All these rocks always contain low content of magnetic minerals. Therefore, due to the lithology of the parent rock, there is a difference in the magnetic mineral concentration ( $\chi_{lf}$ ) between the upper reach and the middle to lower reaches.

#### 4.3 Influences of chemical weathering processes on the river sediment magnetism

The CIA value shows that most samples have experienced moderate- to high-intensity chemical weathering (Fig. 3; Table 1). With the exception of LT-1, the reversed correlation between  $Al_2O_3$  and  $SiO_2$  for all samples indicates the influences of particle size and the quartz addition (Fig. 8a). Generally, samples below the regression line ( $Al_2O_3 = -0.45 SiO_2 + 45$ ) contain Fe-rich sediments, derived from the basalts and metabasalts (Garzanti et al. 2019). The slag of iron ore within LT-1 could be responsible for the distribution of LT-1 in the  $Al_2O_3$  vs  $SiO_2$  plot (Fig. 8a). In general, the WIP and CIA respond very

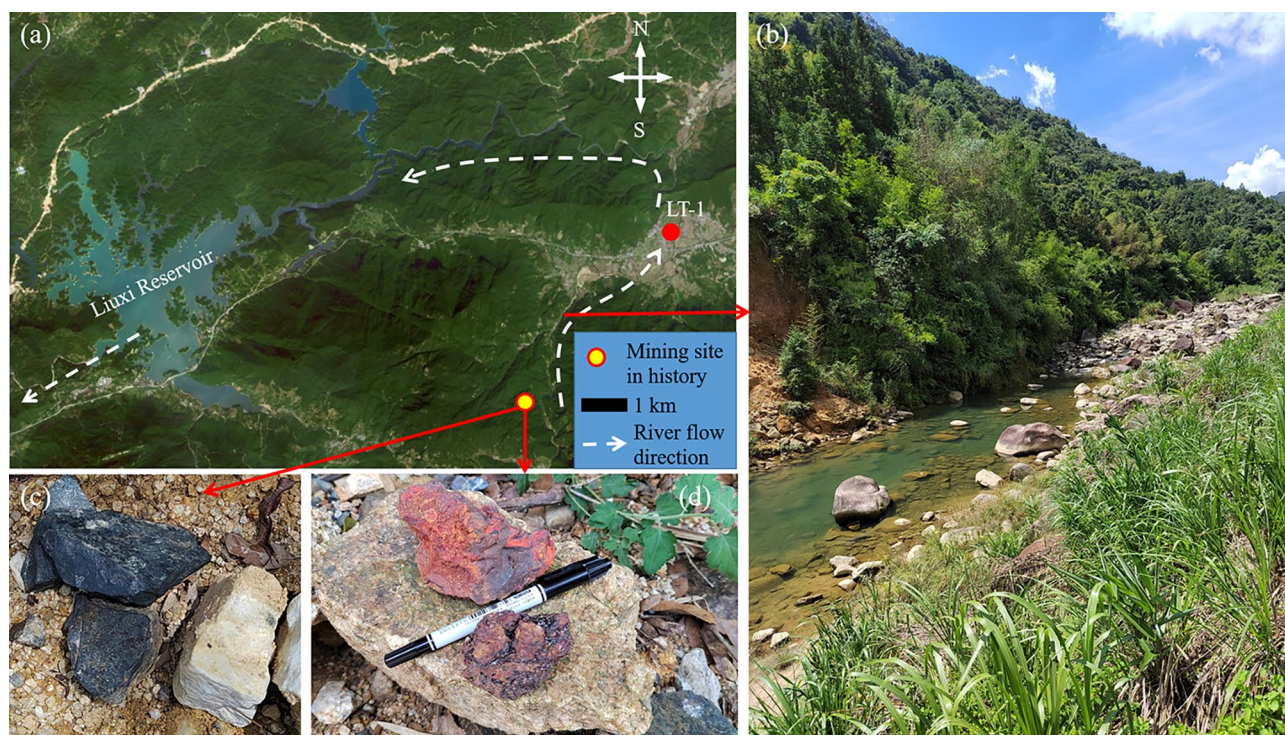


**Fig. 7** **a** Locations of LT-1 and the documented mining sites in history. **b** Landscape of the mountain river between the mining site and the LT-1. The widespread **c** iron ore and **d** slag along the roadside

differently to the sediment recovery, and thus, their relationship can be applied to identify the addition of quartz associated with the recovery (Garzanti et al. 2013). The samples SG-2, JK-2, TP-2, and TP-3 deviate from the CIA–WIP correlation line (Fig. 8b), and the weathering lines in the  $\text{SiO}_2$  and  $\text{Al}_2\text{O}_3$  vs alkali metals (Fig. 8c–d), which implies the existence of recycled fragments from source rocks for four samples (Guo et al. 2018). The phenomenon has been observed in the sand sediments of southern China rivers (He et al. 2020). Notably, these found samples were all retrieved in the downtown and the downstream of the river and close to the barrages (Fig. 1). The construction of barrages may lead to the erosion of soils and the mix of foreign materials, which has promoted the recycling of materials.

There is no correlation between magnetic parameters and CIA though the entire river system (Fig. 3). Interestingly, the parameters related to the high-coercivity magnetic minerals, including HIRM and  $S_{-300}$ , show correlations with the CIA for the samples SG-2, JK-3, TP-2, and TP-3 (Fig. 8e). Different with most samples that have undergone long-term and stable in situ chemical weathering, the recovered materials came from the recycled quartz and the surface's fresh soils for the four samples (Fig. 8b), which was being rapidly eroded by the infrastructure activities. For example, the Conghua Bridge project across the Liuxi River in Jiekou

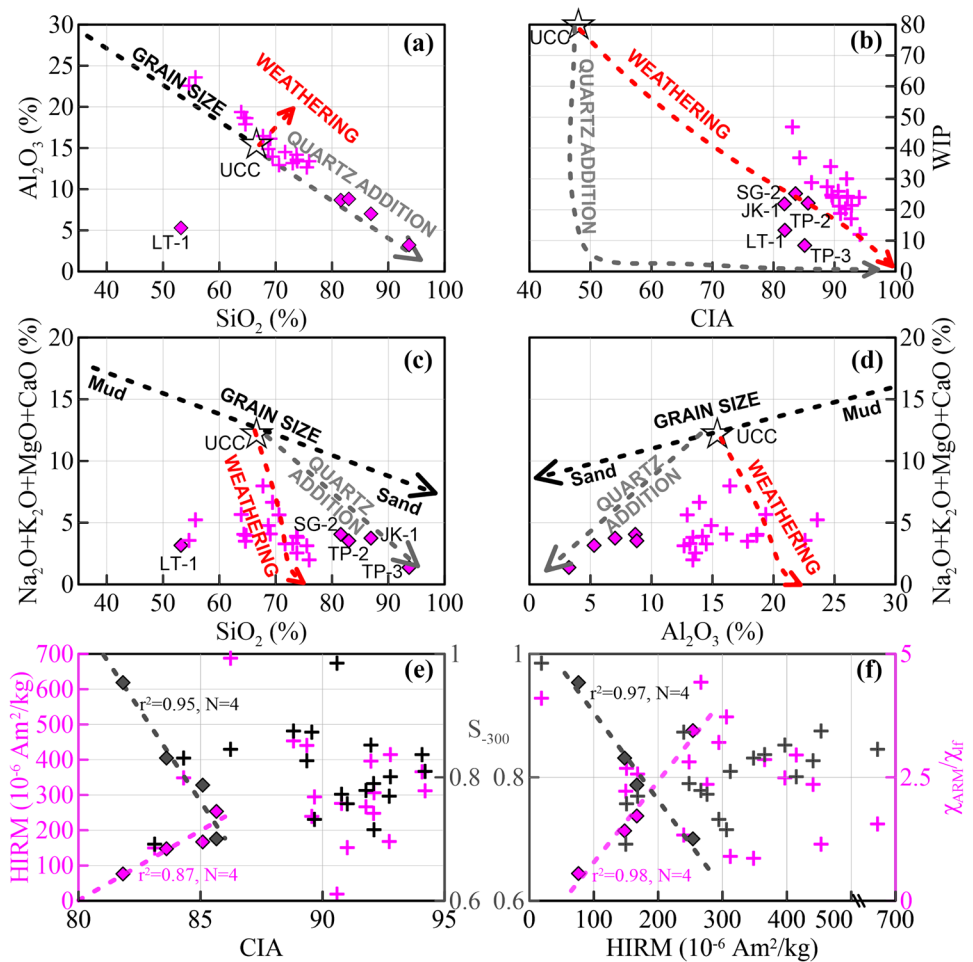
Street of the downtown has been passively constructed since December 2015 (Ning et al. 2016).

As compared with other samples, the sample TP-2 is an extreme case, which contains a high relatively content of high-coercivity minerals (Fig. 4d) and SP particles (Fig. 3e) that derived from fresh soils. During the chemical weathering processes of the surface soils under relatively warm climate, the magnetite and maghemite can be oxidized to hematite and goethite (Jiang et al. 2018; Hu et al. 2020), resulting in higher CIA and HIRM, and lower  $S_{-300}$  values. The rapid burial of fresh soils, carrying the recycled sediments, resulted in the preservation of the correlations of CIA vs. HIRM and CIA vs.  $S_{-300}$ , while other samples were affected by other more factors. Magnetic parameters could be applied to identify the recycling of source materials, because the HIRM is positively correlated with  $\chi_{\text{ARM}}/\chi_{\text{lf}}$ , and negatively correlated with  $S_{-300}$  (Fig. 8f). Only four samples located around the bridges were used in this work, and more samples and models would be conducted to verify the hypothesis in the future research.

#### 4.4 Influences of hydrodynamic sorting on the river sediment magnetism

The tendency of magnetic mineral assemblage to get finer in a downstream direction (Fig. 3f) may result from

**Fig. 8 a–d** Discriminating the control of weathering, recycling, and particle size on the chemical composition of the Liuxi River sediments (diagrams after Garzanti et al. (2019)). Scatter plots of **e** HIRM and  $S_{-300}$  vs. CIA, and **f**  $\chi_{ARM}$  and  $S_{-300}$  vs. HIRM. The Upper Continental Crust standard (UCC) data are from Taylor and McLennan (1985). The empirical lines in (a–d) are from Garzantiet al. (2019)



hydrodynamic sorting, because coarse-grained ferrimagnetic minerals are preferentially deposited upstream and more fine-grained particles are transported downstream (Nguyen et al. 2016; Li et al. 2017; Mzuza et al. 2017). In the upstream Liuxi River (excluding LT-1),  $\chi_{If}$ ,  $\chi_{ARM}$ , SIRM, and HIRM have positive correlation with the coarse silt (32–63  $\mu\text{m}$  fraction) (Fig. 9). This phenomenon is consistent with the results of Li et al. (2017), in which the 32–63  $\mu\text{m}$  fraction was reported as the main carrier of magnetic particles in the Oujiang River, South China. This implies that the coarse silt is a relatively stable magnetic carrier in south China rivers. However, the contents of magnetic particles in the middle and down reaches have no relation with particle sizes, probably because the magnetic particles are controlled by other influencing factors (e.g., human activity and surface runoff from the local catchment) instead of the hydrodynamic sorting.

The sediment magnetic minerals in the river basin are also affected by the barrages in the Liuxi River since the grain size of magnetic minerals becomes coarser, and magnetic concentration becomes higher after flowing through the barrages (Fig. 3). Generally, the barrage blocks the

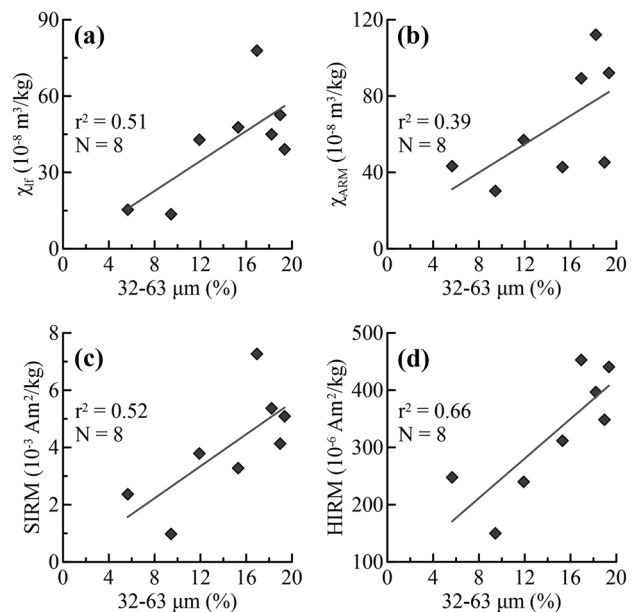


**Fig. 9** Scatter plots between **a**  $\chi_{If}$ , **b**  $\chi_{ARM}$ , **c** SIRM, and **d** HIRM and the content of 32–63  $\mu\text{m}$  in the upstream of the Liuxi River

suspended load from upstream, and thus, most of the suspended load was deposited at the barrage front with the reduction of water velocity (Rákóczi 2010). Downstream of the barrages, more recently eroded materials could be supplied to the river channel, leading to the coarsening of magnetic particles.

#### 4.5 The influences of industrial and resident activities on the river sediment magnetism

The magnetic spherical particles (or so-called technologic magnetic particles) were found in the downtown and downstream reaches of the Liuxi River. One of the final products during coal combustion and other high-temperature burning processes in the blast furnaces is the magnetite-like phase, which appears as single spherule-like grain (McLennan et al. 2000; Sokol et al. 2002; Jordanova et al. 2004; Yang et al. 2007; Lu et al. 2016). There is an industrial park located in the downtown of the river (Jiekou), which is concentrated in the industries of machinery and equipment manufacturing, home appliances manufacturing, medicine/cosmetics,

building materials, etc.. Hence, the emissions from the industrial combustion may lead to the emergence of technologic magnetic particles.

The increase in magnetic contents in the main urban area (JK-6, JK-1, and LK) (Fig. 3a) may be a response to the residents' activities. Similar phenomena have been found in other urban areas, indicating that human activities have a consistent impact on the increased magnetism (Szczepaniak-Wnuk et al. 2020). Although the intensities of human activities are not as strong as that of industrial cities, sediment magnetism in the studied river flowing through small downtown can also provide a significant response to the residents' activities (Zhang et al. 2011). Previous studies suggested that the magnetic method could be applied to quickly delineate potentially high environmental risk areas in catchments (Chaparro et al. 2011; Szczepaniak-Wnuk et al. 2020). However, for small mountain rivers with low-level pollution such as the Liuxi River, it is difficult to characterize the impact of human activities through the increase of magnetic concentration owing to many factors that affect the magnetism of sediments.

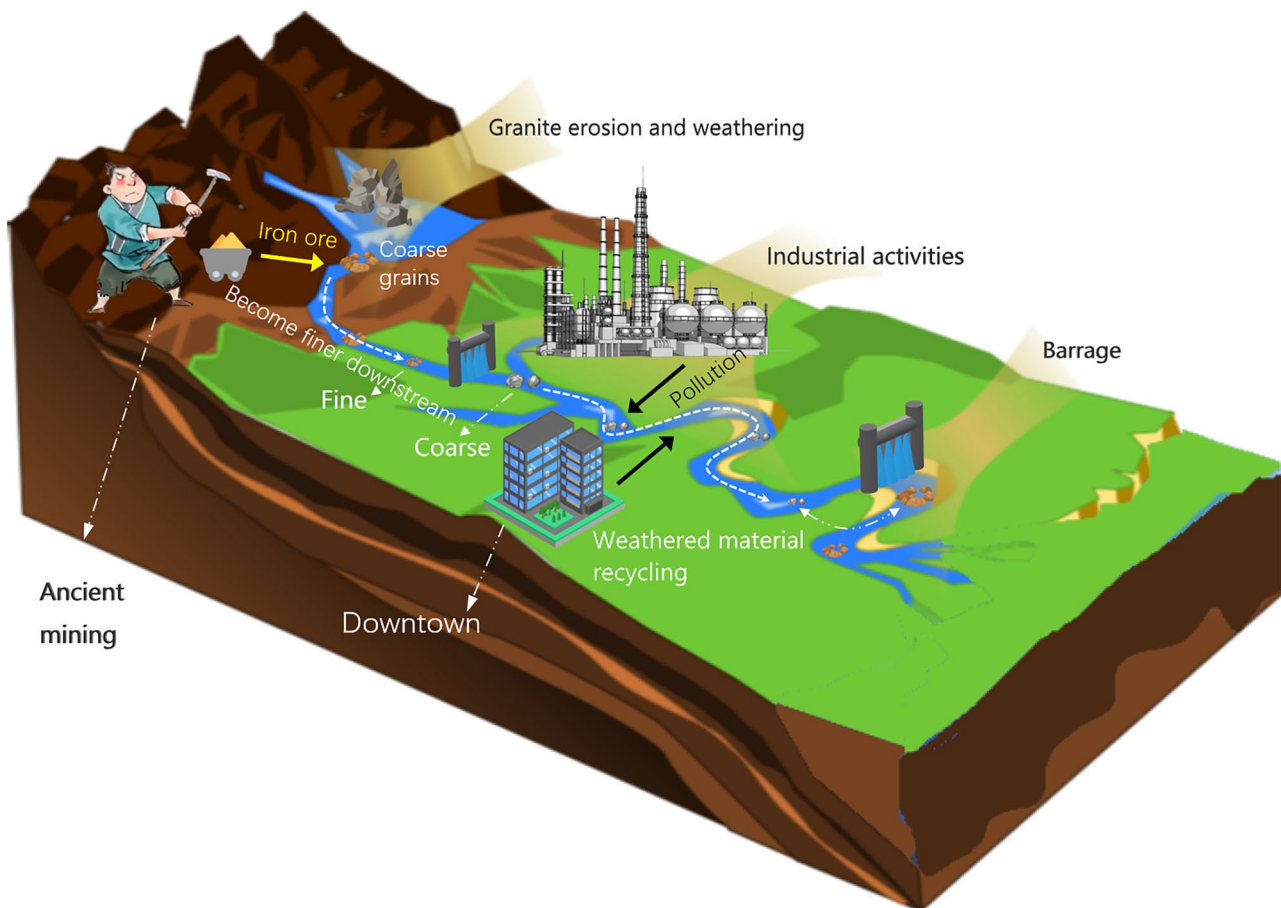


**Fig. 10** Model for magnetic variability in the Liuxi River sediments

## 5 Summary and conclusion

In this work, the sediment magnetic properties in the Liuxi River of subtropical China were found to be affected by several factors:

1. In the upper reach, magnetic susceptibility of the LT-1 is more than 100 times that of other samples. The abnormally high magnetic content is due to the iron ore mining and smelting activities in the area over the past hundreds of years, because the site is located in an outcrop of sedimentary rocks with skarnization. The ancient mining activities still affect the modern river sediment through slag and related metal elements.
2. Magnetic minerals in upstream are mainly characterized as the weakly weathered coarse-grained particles produced by granite denudation, while the magnetic minerals downstream come from the sedimentary rocks imported by human activity. The contributions of SP particles and high-coercivity minerals (e.g., hematite) has increased, and there are technogenic magnetic particles present in the downtown and downstream of the Liuxi River, indicating the anthropogenic influence.
3. Due to hydrodynamic sorting, the magnetic concentration in the downstream of the Liuxi River has decreased, and the magnetic grain size has become finer. After the river passes through the barrages, the magnetic minerals become coarser due to the hydrodynamic changes.
4. Chemical weathering process only plays a key role in sediment magnetism in the regions close to barrages, which may be due to the coupling process of chemical weathering and magnetic mineral oxidation in the freshly eroded soils.

A model concerning the influences of parent rocks, chemical weathering, hydrodynamic sorting, and industrial and resident activities was proposed in Fig. 10. Although the model cannot cover all the change patterns of the magnetic properties in complex rivers, it is helpful to understand the driving factors of the magnetic variability of small mountain rivers. This study emphasizes the strong variability of sediment magnetism in the small river watershed, and more researches are required to deepen the understanding of the sediment magnetic properties in small mountain rivers.

**Acknowledgements** The authors are grateful to Mr. Weitong Xu, Ms. Xueman Wu, and Mr. Min Zeng at South China Normal University for their help in the magnetic measurements. Thanks are given to Dr Philip N. Owens, Dr Simon Pulley and two anonymous reviewers for their helpful comments and suggestions.

**Funding** The study was financially supported by the National Natural Science Foundation of China (41977261), Science and Technology Service Platform Project of GPWREE (cy0603yz02), and Guangdong Natural Science Foundation (2019A1515110195).

## Declarations

**Ethical standard** This article does not contain any studies with human participants performed by any of the authors.

**Conflict of interest** The authors declare no competing interests.

## References

- Bloemendal J, Lamb B, King J (1988) Paleoenvironmental implications of rock magnetic properties of Late Quaternary sediment cores from the eastern equatorial Atlantic. *Paleoceanography* 3(1):61–87
- Chaparro MAE, Chaparro MAE, Rajkumar P, Ramasamy V, Sinito AM (2011) Magnetic parameters, trace elements, and multivariate statistical studies of river sediments from southeastern India: a case study from the Vellar River. *Environ Earth Sci* 63(2):297–310. <https://doi.org/10.1007/s12665-010-0704-2>
- Chaparro MAE, Sinito AM, Ramasamy V, Marinelli C, Chaparro MAE, Mullainathan S, Murugesan S (2008) Magnetic measurements and pollutants of sediments from Cauvery and Palaru River. *India Environ Geol* 56(2):425–437. <https://doi.org/10.1007/s00254-007-1180-1>
- Deng K, Yang S, Bi L, Chang YP, Su N, Frings P, Xie X (2019) Small dynamic mountainous rivers in Taiwan exhibit large sedimentary geochemical and provenance heterogeneity over multi-spatial scales. *Earth Planet Sci Lett* 505:96–109. <https://doi.org/10.1016/j.epsl.2018.10.012>
- Dong C, Zhang W, He Q, Dong Y, Yu L (2014) Magnetic fingerprinting of hydrodynamic variations and channel erosion across the turbidity maximum zone of the Yangtze Estuary, China. *Geomorphology* 226:300–311. <https://doi.org/10.1016/j.geomorph.2014.08.008>
- Franke C, Kissel C, Robin E, Bonté P, Lagroix F (2009) Magnetic particle characterization in the Seine river system: implications for the determination of natural versus anthropogenic input. *Geochem Geophys Geosy* 10(8). <https://doi.org/10.1029/2009gc002544>
- Garzanti E, Andò S, France-Lanord C, Vezzoli G, Censi P, Galy V, Najman Y (2010) Mineralogical and chemical variability of fluvial sediments: 1. Bedload sand (Ganga–Brahmaputra, Bangladesh). *Earth Planet Sci Lett* 299(3–4):368–381. <https://doi.org/10.1016/j.epsl.2010.09.017>
- Garzanti E, Padoan M, Andò S, Resentini A, Vezzoli G, Lustrino M (2013) Weathering and relative durability of detrital minerals in equatorial climate: sand petrology and geochemistry in the East African Rift. *J Geol* 121(6):547–580. <https://doi.org/10.1086/673259>
- Garzanti E, Vermeesch P, Vezzoli G, Andò S, Botti E, Limonta M, Dinis P, Hahn A, Baudet D, De Grave J (2019) Congo River sand and the equatorial quartz factory. *Earth-Sci Rev* 197:102918. <https://doi.org/10.1016/j.earscirev.2019.102918>
- Garzanti E, He J, Barbarano M, Resentini A, Li C, Yang L, Yang S, Wang H (2021) Provenance versus weathering control on sediment composition in tropical monsoonal climate (South China)- 2. Sand petrology and heavy minerals. *Chem Geol* 564:119997. <https://doi.org/10.1016/j.chemgeo.2020.119997>
- Guangdong Geological Survey (2000) Regional geological survey report of Guangzhou (1:250000). (in Chinese)
- Guo Y, Yang S, Su N, Li C, Yin P, Wang Z (2018) Revisiting the effects of hydrodynamic sorting and sedimentary recycling on chemical weathering indices. *Geochim Cosmochim Acta* 227:48–63. <https://doi.org/10.1016/j.gca.2018.02.015>

- He J, Garzanti E, Dinis P, Yang S, Wang H (2020) Provenance versus weathering control on sediment composition in tropical monsoonal climate (South China)-I. Geochemistry and Clay Mineralogy. *Chem Geol* 558:119860. <https://doi.org/10.1016/j.chemgeo.2020.119860>
- Hong C, Huh C, Chen K, Huang P, Hsiung K, Lin H (2009) Air pollution history elucidated from anthropogenic spherules and their magnetic signatures in marine sediments offshore of Southwestern Taiwan. *J Marine Syst* 76(4):468–478. <https://doi.org/10.1016/j.jmarsys.2007.09.014>
- Hu P, Heslop D, Rossel RAV, Roberts AP, Zhao X (2020) Continental-scale magnetic properties of surficial Australian soils. *Earth-Sci Rev* 203:103028. <https://doi.org/10.1016/j.earscirev.2019.103028>
- Huang X, Zhao L (2017) Preliminary survey and protection measures research of water environment conditions of Liuxi river valley in Guangzhou city. *Guangzhou Environmental Science* 111–115. (in Chinese with English Abstract)
- Ji DQ, Wen Y, Wei JB, Wu ZF, Cheng J, Liu Q (2013) Dynamic trend of land use landscape ecological security in Liuxihe watershed. *Trop Geo* 33:299–306. (in Chinese with English Abstract)
- Jian X, Yang S, Hong D, Liang H, Zhang S, Fu H, Zhang W (2020) Seasonal geochemical heterogeneity of sediments from a subtropical mountainous river in SE China. *Mar Geol* 422:106120. <https://doi.org/10.1016/j.margeo.2020.106120>
- Jiang Z, Liu Q, Roberts AP, Barrón V, Torrent J, Zhang Q (2018) A new model for transformation of ferrihydrite to hematite in soils and sediments. *Geology* 46:987–990. <https://doi.org/10.1130/g45386.1>
- Jordanova D, Hoffmann V, Fehr KT (2004) Mineral magnetic characterization of anthropogenic magnetic phases in the Danube river sediments (Bulgarian part). *Earth Planet Sci Lett* 221(1–4):71–89. [https://doi.org/10.1016/s0012-821x\(04\)00074-3](https://doi.org/10.1016/s0012-821x(04)00074-3)
- Koiter AJ, Owens PN, Petticrew EL, Lobb DA (2013) The behavioural characteristics of sediment properties and their implications for sediment fingerprinting as an approach for identifying sediment sources in river basins. *Earth-Sci Rev* 125:24–42. <https://doi.org/10.1016/j.earscirev.2013.05.009>
- Li L (1979) Capitalism in embryo of Guangdong mining and smelting industry in the early Qing Dynasty. *Aust Acad Res Libr* 5:116–127. (in Chinese)
- Li Y (2020) Spatial distribution and influencing factors of urban and rural settlements in Liuxi river basin. *Geomatics Spatial Inform Tech* 43:111–115. (in Chinese with English Abstract)
- Li M, Chen W, Ouyang T, He C, Kuang Y, Peng S (2021) The impact of energetic tropical cyclones (typhoons) on the modern sediment magnetism along the South China coast. *Cont Shelf Res* 224:104447. <https://doi.org/10.1016/j.csr.2021.104447>
- Li W, Hu Z, Zhang W, Ji R, Nguyen TTH (2017) Influence of provenance and hydrodynamic sorting on the magnetic properties and geochemistry of sediments of the Oujiang River, China. *Mar Geol* 387:1–11. <https://doi.org/10.1016/j.margeo.2017.03.002>
- Liu Z, Ma J, Wei G, Liu Q, Jiang Z, Ding X, Peng S, Zeng T, Ouyang T (2017) Magnetism of a red soil core derived from basalt, northern Hainan Island, China: volcanic ash versus pedogenesis. *J Geophys Res-Sol Ea* 122:1677–1696. <https://doi.org/10.1002/2016jb013834>
- Lu S, Yu X, Chen Y (2016) Magnetic properties, microstructure and mineralogical phases of technogenic magnetic particles (TMPs) in urban soils: their source identification and environmental implications. *Sci Total Environ* 543:239–247. <https://doi.org/10.1016/j.scitotenv.2015.11.046>
- Luo J (2005) Geological characteristics of Gutian Iron Mine in Conghua City, Guangdong Province. *West-China Explor Eng* 113(9):91–92. (in Chinese)
- Lynch M (2003) Mining in world history. Reaktion Books
- Mariyanto M, Amir MF, Utama W, Hamdan AM, Bijaksana S, Pratama A, Yunginger R, Sudarningsih S (2019) Heavy metal contents and magnetic properties of surface sediments in volcanic and tropical environment from Brantas River, Jawa Timur Province, Indonesia. *Sci Total Environ* 675:632–641. <https://doi.org/10.1016/j.scitotenv.2019.04.244>
- McLennan A, Bryant G, Stanmore B, Wall T (2000) Ash formation mechanisms during pf combustion in reducing conditions. *Energy Fuel* 14(1):150–159. <https://doi.org/10.1021/ef990095u>
- Milliman JD, Farnsworth KL (2011) River discharge to the coastal ocean: a global synthesis. Cambridge University Press, Cambridge
- Moon S, Huh Y, Qin J, van Pho N (2007) Chemical weathering in the Hong (Red) River basin: rates of silicate weathering and their controlling factors. *Geochim Cosmochim Acta* 71(6):1411–1430. <https://doi.org/10.1016/j.gca.2006.12.004>
- Mzuzza MK, Zhang W, Kapute F, Selemani JR (2017) Magnetic properties of sediments from the Pangani River Basin, Tanzania: influence of lithology and particle size. *J Appl Geophys* 143:42–49. <https://doi.org/10.1016/j.jappgeo.2017.05.015>
- Nesbitt HW, Young GM (1982) Early Proterozoic climates and plate motions inferred from major element chemistry of lutites. *Nature* 299:715–717
- Nguyen HTT, Zhang W, Li Z, Li J, Ge C, Liu J, Bai X, Feng H, Yu L (2016) Magnetic properties of sediments of the Red River, Vietnam: effect of sorting on the source-to-sink pathway and its implications for environmental reconstruction. *Geochem Geophys Geosy* 17(2):270–281. <https://doi.org/10.1002/2015gc006089>
- Ning P, Guo Y (2016) Structural design and key technologies of the spatial arch and girder combined bridge of the main span of the Guangzhou Conghua bridge project. *Urban Roads Bridges & Flood Control* 9:43–45,55. <https://doi.org/10.16799/j.cnki.csdqyf.2016.09.010>
- Oldfield F, Barnosky C, Leopold EB, Smith JP (1983) Mineral magnetic studies of lake sediments. *Hydrobiologia* 103:37–44
- Parker A (1970) An index of weathering for silicate rocks. *Geol Mag* 107:501–504
- Panwar S, Yang S, Srivastava P, Khan M, Sangode S, Chakrapani G (2020) Environmental magnetic characterization of the Alaknanda and Ramganga river sediments, Ganga basin. *India Catena* 190:104529. <https://doi.org/10.1016/j.catena.2020.104529>
- Peters C, Thompson R (1998) Magnetic identification of selected natural iron oxides and sulphides. *J Magn Mater* 183(3):365–374. [https://doi.org/10.1016/s0304-8853\(97\)01097-4](https://doi.org/10.1016/s0304-8853(97)01097-4)
- Pike CR, Roberts AP, Verosub KL (1999) Characterizing interactions in fine magnetic particle systems using first order reversal curves. *J Appl Phys* 85(9):6660–6667. <https://doi.org/10.1063/1.370176>
- Pulley S, Lagesse J, Ellery W (2017) The mineral magnetic signatures of fire in the Krom River wetland. *South Africa J Soils Sediments* 17(4):1170–1181. <https://doi.org/10.1007/s11368-016-1577-0>
- Rákóczi L (2010) Sediment regime of the River Danube (1956–1985): hydrological processes of the Danube River basin. Springer, Dordrecht, pp 293–304. [https://doi.org/10.1007/978-90-481-3423-6\\_9](https://doi.org/10.1007/978-90-481-3423-6_9)
- Roberts AP, Heslop D, Zhao X, Pike CR (2015) Understanding fine magnetic particle systems through use of first-order reversal curve diagrams. *Rev Geophys* 52(4):557–602. <https://doi.org/10.1002/2014rg000462>
- Roberts AP, Pike CR, Verosub KL (2000) First-order reversal curve diagrams: a new tool for characterizing the magnetic properties of natural samples. *J Geophys Res* 105(B12):28461–28475. <https://doi.org/10.1029/2000jb900326>
- Roberts AP, Zhao X, Harrison RJ, Heslop D, Muxworthy AR, Rowan CJ, Larrasoana JC, Florindo F (2018) Signatures of reductive magnetic mineral diagenesis from unmixing of first-order reversal curves. *J Geophys Res-Sol Ea* 123(6):4500–4522. <https://doi.org/10.1029/2018jb015706>
- Shao J, Yang S, Li C (2012) Chemical indices (CIA and WIP) as proxies for integrated chemical weathering in China: inferences from

- analysis of fluvial sediments. *Sediment Geol* 265–266:110–120. <https://doi.org/10.1016/j.sedgeo.2012.03.020>
- Shen M, Zan J, Yan M, Zhang W, Fang X, Zhang D, Zhang T (2020) Comparative rock magnetic study of Eocene volcanogenic and sedimentary rocks from Yunnan, southeastern Tibetan Plateau, and its geological implications. *J Geophys Res-Sol Ea* 125(2). <https://doi.org/10.1029/2019jb017946>
- Shepard FP (1954) Nomenclature based on sand-silt-clay ratios. *J Sediment Res* 24:151–158. <https://doi.org/10.1306/d4269774-2b26-11d7-8648000102c1865d>
- Sokol E, Kalugin V, Nigmatulina E, Volkova N, Frenkel A, Maksimova N (2002) Ferrospheres from fly ashes of Chelyabinsk coals: chemical composition, morphology and formation conditions. *Fuel* 81(7):867–876. [https://doi.org/10.1016/s0016-2361\(02\)00005-4](https://doi.org/10.1016/s0016-2361(02)00005-4)
- Steffen W, Sanderson RA, Tyson PD, Jäger J, Matson PA, Moore IIIB, Oldfield F, Richardson K, Schellnhuber HJ, Turner BL (2006) *Global change and the earth system: a planet under pressure*. Springer Science & Business Media
- Su N, Yang S, Guo Y, Yue W, Wang X, Yin P, Huang X (2017) Revisit of rare earth element fractionation during chemical weathering and river sediment transport. *Geochem Geophys Geosy* 18(3):935–955. <https://doi.org/10.1002/2016gc006659>
- Sudarningsih S, Maulana L, Bijaksana S, Hafidz A, Pratama A, Widodo W, Iskandar I (2017) Magnetic characterization of sand and boulder samples from Citarum River and their origin. *J Math Fundam Sci* 49(2):116. <https://doi.org/10.5614/j.math.fund.sci.2017.49.2.2>
- Szczepaniak-Wnuk I, Górka-Kostrubiec B, Dytłow S, Szwarczewski P, Kwapuliński P, Karasiński J (2020) Assessment of heavy metal pollution in Vistula river (Poland) sediments by using magnetic methods. *Environ Sci Pollut R* 27(19):24129–24144. <https://doi.org/10.1007/s11356-020-08608-4>
- Taylor SR, McLennan SM (1985) *The continental crust: its composition and evolution*. Blackwell, London
- Warrier AK, Sebastian JG, Amrutha K, Sali AY, Mahesh BS, Mohan R (2021) Magnetic properties of surface sediments in Schirmacher Oasis, East Antarctica: spatial distribution and controlling factors. *J Soils Sediments* 21(2):1206–1221. <https://doi.org/10.1007/s11368-020-02824-8>
- Yang D, Wang M, Liu J, Deng T, Yan C, Ding Z, Lu H (2020) Occurrence and characteristics of iron-bearing minerals in surface road dusts: a case study in the coastal areas of southern Fujian, China. *J Soils Sediments* 20(9):3406–3416. <https://doi.org/10.1007/s11368-020-02667-3>
- Yang T, Liu Q, Chan L, Liu Z (2007) Magnetic signature of heavy metals pollution of sediments: case study from the East Lake in Wuhan. *China Environ Geol* 52(8):1639–1650. <https://doi.org/10.1007/s00254-006-0609-2>
- Zhang C, Qiao Q, Piper JDA, Huang B (2011) Assessment of heavy metal pollution from a Fe-smelting plant in urban river sediments using environmental magnetic and geochemical methods. *Environ Pollut* 159(10):3057–3070. <https://doi.org/10.1016/j.envpol.2011.04.006>
- Zhang Q, Appel E, Hu S, Pennington RS, Meyer J, Neumann U, Koutsodendris A (2020) Nano-magnetite aggregates in red soil on low magnetic bedrock, their changes during source-sink transfer, and implications for paleoclimate studies. *J Geophys Res-Sol Ea* 125(10):e2020JB020588. <https://doi.org/10.1029/2020JB020588>
- Zhang Q, Liu Q, Li J, Sun Y (2018) An integrated study of the eolian dust in pelagic sediments from the North Pacific Ocean based on environmental magnetism, transmission electron microscopy, and diffuse reflectance spectroscopy. *J Geophys Res-Sol Ea* 123(5):3358–3376. <https://doi.org/10.1002/2017jb014951>

**Publisher's Note** Springer Nature remains neutral with regard to jurisdictional claims in published maps and institutional affiliations.